PERGAMON

International Journal of Multiphase Flow 27 (2001) 1769–1787

International Journal of Multiphase Flow

www.elsevier.com/locate/ijmulflow

Measurement of air-entrainment from a stationary Taylor bubble in a vertical tube

R. Delfos [a,*], C.J. Wisse [a], R.V.A. Oliemans [b]

[a] *Laboratory for Aero- and Hydrodynamics, J.M. Burgers Centre for Fluid Mechanics, Delft University of Technology, Leeghwaterstraat 21, NL-2628 CB Delft, Netherlands*

[b] *Kramers Laboratory for Physical Technology, Netherlands*

Received 19 July 1998; received in revised form 29 March 2001

Abstract

To get insight into the air entrainment process from a Taylor bubble in a vertical tube, we measured the gas loss from a Taylor bubble that was held stationary in a downward liquid flow. Also, we measured the void fraction in the downward bubbly flow below the Taylor bubble, as well as the radial void fraction distribution in this region. We varied the Taylor bubble length, the liquid flow rate approaching the bubble, and the turbulence level of this flow. The experiments strongly indicate that the entrainment flux is related to the presence of turbulence in the liquid film surrounding the Taylor bubble. © 2001 Elsevier Science Ltd. All rights reserved.

Keywords: Two-phase flow; Vertical slug flow; Taylor bubble; Film flow; Entrainment; Void fraction; Bubbly flow; Film surface

1. Introduction

Taylor bubbles are (gas) bubbles in a vertical tube, that are so large that they nearly completely span the tube diameter, D. These bubbles are commonly found in many industrial flows like inside heat exchangers, furnaces or oil production tubing, but they are also found in everyday life environment like in a coffee percolator. In all these cases there is a vertical upward two-phase flow; the flow pattern is called slug flow.

During slug flow in a vertical tube, Taylor bubbles rise more or less steadily through slugs of liquid that are in most cases loaded with small dispersed gas bubbles. An important role in

* Corresponding author.
E-mail address: r.delfos@wbmt.tudelft.nl (R. Delfos).

0301-9322/01/$ - see front matter © 2001 Elsevier Science Ltd. All rights reserved.
PII: S0301-9322(01)00029-5

predicting the pressure drop and the stability of the flow pattern is played by the volume fraction of gas in a slug α, also known as the void fraction, or the gas hold-up. When α exceeds a certain level (0.25–0.3), the bubbles have a large probability to coalesce and a transition to churn flow or annular flow will follow. Models are presented, among others, by Taitel et al. (1980); measurements are presented, among others, by van Hout et al. (1992). Since measurements show relatively narrow distributions of slug length and Taylor bubble length (Mao and Dukler, 1989), slug flow is commonly treated as an exactly periodic flow. Various so-called slug-unit flow models exist nowadays that determine α from physical quantities of the flow (among others Fernandes et al., 1983 and Dukler and Fabre, 1992, give an overview). Also, attempts have been made to model instationary slug flow (Fabre et al., 1989).

Fernandes et al. (1983) determine α from the liquid and the gas flow rates, the physical properties of the fluids and the geometry. Closure models are needed for the fluxes of gas and liquid into and out of the slug that are shown in Fig. 1.

- At the lower end, the mixture in the slug is overtaken by the Taylor bubble below. The gas is considered to coalesce with the Taylor bubble (flux Φ_A); the liquid falls as a film around the bubble (flux Φ_L).
- At the top, a slug gains liquid (flux Φ_L) from the film running down around the Taylor bubble above it. With this film, gas can be swept from the Taylor bubble into the slug to form small bubbles, the so-called entrainment flux Φ_C.
- Part of these bubbles may re-coalesce with the Taylor bubble in its wake (flux Φ_B); the others are dispersed into the slug.

The underlying physical mechanisms for the entrainment and the re-coalescence processes are not fully understood. As a result, a proper closure is difficult to find. Fernandes et al. (1983) and Andreussi and Bendiksen (1989) close their slug flow models, for vertical and for horizontal flow, respectively. The latter authors define a minimum film velocity below which no bubbles are

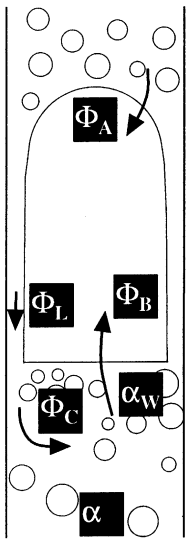

Fig. 1. Gas balance of a Taylor bubble in slug flow.

produced. Oliemans (1990) has extended the Andreussi-model for any tube inclination. This gives a gas hold-up for vertical slug flow that increases with the mixture velocity, qualitatively agreeing with experiments. In all these slug flow models, sub-models for the entrainment and the re-coalescence rates are given. Unfortunately these models are not capable of predicting the characteristics of slug flow with sufficient accuracy, as was shown, among others, in a review paper by Dukler and Fabre (1992). In contrast with these models, simplified data correlations for α contain little physics but are relatively accurate for the parameter range they were made for. As a consequence, in slug flow models such correlations are often still in use.

Our study is directed to get more insight into the physical mechanisms of gas entrainment and re-coalescence, which could lead to a better prediction of the gas flows related to these processes. To this end, we concentrate on the gas exchange process during slug flow by performing experiments on a standing Taylor bubble; a single bubble that is held stationary in a downward water flow. Here we will present measurements of the rate of air loss from the Taylor bubble, which for stationary flow is equal to the entrainment Φ_C minus the re-coalescence Φ_B. Clearly this flow situation is not completely identical to that of upward slug flow, where the tube wall is running downward relative to the slug. In that case, the film velocity relative to the slug will be much higher than in our flow. Also, the turbulence level inside the slug will differ from ours, likely influencing the dispersion process in the Taylor bubble wake. Consequently, our data cannot be compared directly with those measured under slug flow conditions, but they can be used to develop models for the entrainment and the re-coalescence. Such models, when based on the proper parameters, can then be applied as gas-transfer relations in a slug flow model. To avoid confusion, we will further on use the term 'liquid column' instead of 'liquid slug' for the liquid below a standing Taylor bubble in our experiment.

Various similar experiments on air entrainment behind a stagnant bubble have been presented in the literature. The similarities and differences compared to our experiment can be described as follows:

- Riiser et al. (1992) made water flow downward through a $D = 51$ mm pipe around a centred massive cylinder of $0.8D$. When air is injected below the cylinder through a centred bore in it, the $0.1D$ thick surrounding annular liquid jet forms a wall film flow before impinging into the liquid column below.
- Bacon et al. (1995) injected air into a downward pipe flow ($D = 58$ mm) from, among other geometries, a downwards-pointing centred tubelet of $0.12D$. With a sufficiently high water velocity, a stable cavity forms itself below the tubelet, similar to that in Riiser's experiment. For low water flow rates this cavity was shown to be unstable.
- Su and Metcalfe (1997) produced standing bubbles in a downward pipe flow ($D = 51$ mm) by blowing air from a centred tube of $0.37D$. They investigated the influence of the water properties by using additives to increase the viscosity and to lower the surface tension.

In our experiment, on which some first crude data were presented in Delfos et al. (1993), we have chosen to study entrainment and coalescence at a Taylor-bubble-shaped air cavity in a much larger tube ($D = 100$ mm). This diameter was chosen such that there is a relatively large difference between the free rise velocity of a Taylor bubble, U_0, and that of small dispersed bubbles in a slug below a Taylor bubble. The latter is typically 0.20–0.25 m/s in water over a large range of bubble diameters, see for instance Wallis (1969). However, U_0 does depend on the tube diameter (see

Section 2.2 later on). In a small diameter tube, such as that used by Bacon, we find using (1) that $U_0 = 0.26$ m/s; that used by Riiser and by Su gives $U_0 = 0.24$ m/s. Both are nearly equal to that of the dispersed bubbles, which may give rise to the problem that entrained bubbles may not escape from the wake of the slug, and consequently re-coalesce with it. Taitel et al. (1980) suggest to call such flows in small diameter tubes *plug* flow. We have overcome this re-coalescence problem by choosing a much wider tube, for which we get $U_0 = 0.35$ m/s, which makes a difference of at least 0.1 m/s to sweep entrained bubbles away from the Taylor bubble. Therefore re-coalescence may be more easy to separate from entrainment when modelling our flow.

In all three literature papers, data were presented on the entrainment of air from the *bottom* of the cavity as a function of cavity length for various liquid flow rates. Those by Riiser are quite limited; those by Bacon and by Su are more elaborate. In contrast to these experiments, we have given much attention to mimic with our cavity the *nose* side of a Taylor bubble, and we will show in this paper that it has a large influence on the entrainment process. Like in the other three papers, we have measured the gas loss from the fixed Taylor bubble. In addition, we obtained information on the axial and radial distribution of small gas bubbles below the Taylor bubble.

We have manipulated the liquid flow upstream of the bubble to control, besides the liquid flow rate, also both the velocity profile and the turbulence level. With these parameters, we are able to simulate the flow parameters relevant to the Taylor bubble as they would occur during upward slug flow. There is yet a large difference between Taylor bubbles in upward and in downward flows. Martin (1976) showed that the rise velocity of such a bubble in a downward liquid flow deviates strongly from the 'Nicklin law' (see Section 2.2). He explained this from the fact that the bubble nose becomes asymmetric due to the disadvantageous velocity profile upstream of it. In a large tube diameter, he showed that the bubble nose tends to creep into the boundary layer of the liquid flow, and take a completely different shape, and show very unsteady motion. To overcome such problems, in our experiment we stabilise the bubble in the centre of the tube not only by controlling the velocity profile but we also fix the nose of the bubble by using a small cap from which the bubble's free surface emerges. We inject air below this cap through a thin centred tubelet. In Section 3 we will show the good resemblance between a real Taylor bubble and the air cavity we form below this small cap.

In Section 2.2 we will show that there is a liquid flow rate that simulates a Taylor bubble rising through stagnant (non-flowing) liquid. We consider this situation as very important from a fundamental point of view, even though it is not typical for slug flow. In the three previously discussed experiments the liquid flow rates used were in fact much larger than this (minimum) value. In this way they overcome the re-coalescence problem mentioned before. Furthermore, we show that with a small increase of liquid flow, we simulate a much faster flowing 'real' slug flow. Secondly, we will demonstrate in Section 4 that the flow conditions upstream of the Taylor bubble have a very large influence on the entrainment rate, especially for short Taylor bubbles.

After a brief introduction to the experimental set-up and the flow conditions of the Taylor bubble in Section 2, we will present in Section 3 some qualitative observations. In Section 4, we will present our measurements of gas loss and gas distribution in the liquid column below the bubble as a function of Taylor bubble length, liquid flow rate and turbulence level. In Section 5 we will discuss our results.

2. Experimental set-up

2.1. Experimental facility

Our experiments were performed in the SLUG-facility that is shown schematically in Fig. 2. Water is flowing downwards in a vertical tube with inner diameter $D = 99.7$ ($\Delta D = 0.2$ mm), in which air is blown through centred tubelets of outer diameter $0.03D$ (for $U_{SG} < 30$ mm/s) and $0.08D$ (for larger gas flow rates). At the end of the tubelet a small spherically shaped Teflon cap is attached, which is 5 mm thick. The radius of curvature ($0.35D$) is that of a theoretical Taylor bubble nose as is calculated among others by Dumitrescu (1943). Some more details are described at the end of the next paragraph.

The liquid flow rate is adjusted such that a stable Taylor bubble emerges. The liquid film falling down along the bubble runs into the liquid column below it and eventually entrains gas. In Fig. 3 we compare a free rising Taylor bubble with one captured in our set-up. We see that the shape is the same for both bubbles, which suggests that we have a good experimental simulation of the nose of the Taylor bubble. We consider this to be important, since the liquid film is expected to be sensitive to the inlet conditions.

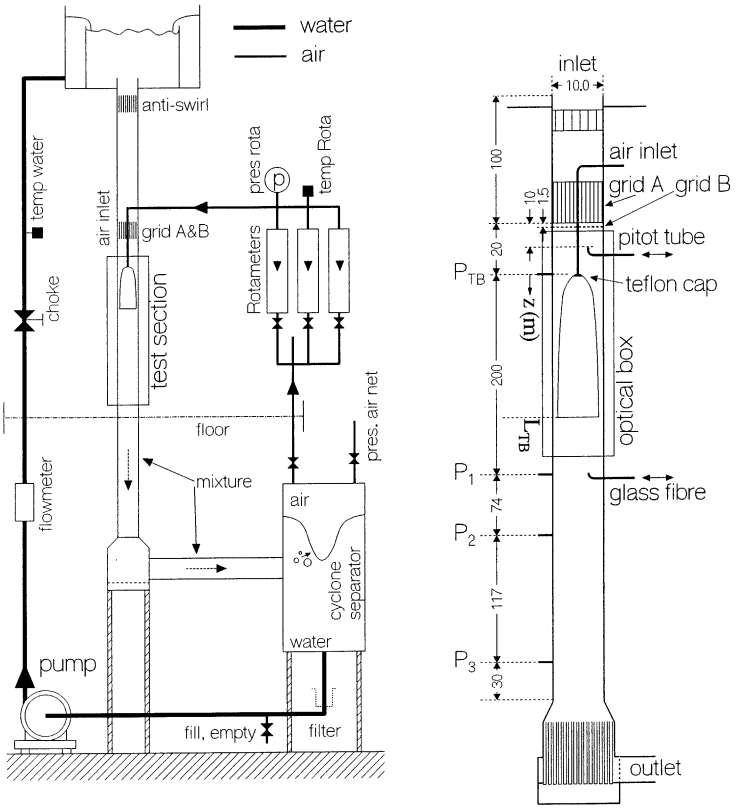

Fig. 2. The SLUG-facility schematically. On the right the 5.5 m high test section is shown, with all dimensions in cm.

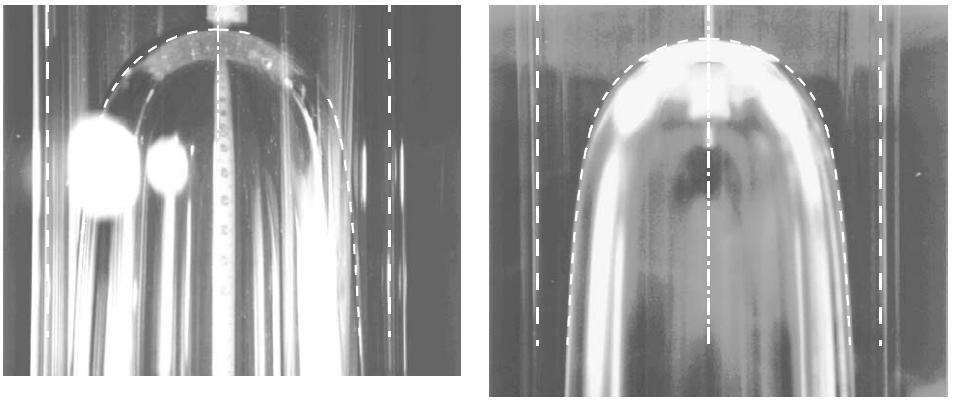

Fig. 3. Two Taylor bubbles: free rising in stagnant liquid (a) and below the white cap (b) in a downflow. The broken line is the theoretical bubble shape.

The liquid velocity U_{SL} is measured by an electro-magnetic flowmeter ($\Delta U_{SL} = 3$ mm/s), mounted in the upward single-phase leg, which also controls the centrifugal pump that drives the flow loop. The air is recirculating in the system. This air flow is driven by the pressure difference between the separator and the air inlet.

The basic quantity measured is the gas flow blown into the Taylor bubble. This volume flow rate, expressed as superficial gas velocity U_{SG}, is measured using three Rota-meters ($\Delta U_{SG} =$ 1.5 mm/s). The value is corrected for the pressure of the Taylor bubble (P_{TB}), as measured at the wall as indicated in Fig. 2.

From pressure measurements we derived the void fraction in the liquid column below the Taylor bubble, $\alpha(z)$. Here void fraction α means the cross-section averaged local void fraction at a certain axial position z below the Taylor bubble nose. There are two important considerations: firstly, the first part of the downward bubbly flow in the slug is a developing flow, starting from a wake with recirculating eddies towards the quasi-fully developed flow described above. The void fraction in the Taylor bubble wake, α_w, is considerably higher than that a few diameters D lower, as was measured, among others, by van Hout et al. (1992) or can be observed from the photographs in Fig. 5 in Section 3. Detailed measurements of the local void fraction distribution in the Taylor bubble wake in upward slug flow by van Hout et al. (1992) showed that already after $10D$, a fully developed bubbly flow has established itself, probably due to the thorough mixing in the wake of the bubble. Secondly, since in our case the bubbles are slowly compressed on their way down because of hydrostatic pressure, the void fraction is not constant in the tube, but decreases slowly in the downflow direction. We are interested in $\alpha(z = L_{TB})$, which is the void fraction just below the Taylor bubble where the partial re-coalescence of the entrained bubbles takes place. In the liquid column below the Taylor bubble, we measured differential pressures (with an accuracy of $\Delta P = 3$ Pa) between three positions (P_1–P_3, indicated in Fig. 2) along the bubbly flow region. We use the one-dimensional drift-flux model (Wallis, 1969) to calculate the void fraction profile $\alpha(z)$ and (by integration) the pressure profile $p(z)$ from the pressure data at P_1 and P_3 and the known fluxes U_{SL} and U_{SG}. The Blasius relation for smooth-walled single-phase pipe flow with the actual liquid velocity was used to account for the wall friction. The error due to this simplification

is rather small because of the low flow velocities used. The distribution parameter in the drift-flux model, C_0, was determined from the data. The model result for $p(z(P_2))$ was checked with the measured value P_2, and found to be typically within 10 Pa accuracy. The accuracy in α was estimated as $\Delta\alpha = 0.002$. Finally, the void fraction below the Taylor bubble $\alpha(z = L_{TB})$, is extrapolated from the model, with $\Delta\alpha(z = L_{TB}) = 0.002$. For Taylor bubbles beyond 1 m length, pressure tap P_1 is less than $10D$ below the Taylor bubble. In that case only the lower two pressure taps P_2 and P_3 were used without a check value. Further details on the applied methods can be found in Delfos (1996).

2.2. Flow conditions procedure

The downward liquid velocity in the set-up can be freely varied; however, only under a limited range of conditions a stable stagnant bubble can be created. This range is related to the relative velocity of the stagnant bubble and the liquid. To investigate this, we will first describe a Taylor bubble rising upward through stagnant or co-flowing liquid, as it is the case during upward slug flow. The velocity of such a bubble, U_{TB}, can be expressed as follows (Nicklin et al., 1962):

$$U_{TB} = 0.35\sqrt{gD} + C_{TB}U_L = U_0 + C_{TB}U_L \quad \text{with} \quad C_{TB} \approx 1.2, \tag{1}$$

where D is the tube diameter, g the gravity acceleration and U_L is the liquid velocity. U_0 is the rise velocity of a Taylor bubble in stagnant liquid. In (1) gravity-dominated flow is assumed, neglecting the influence of surface tension and viscosity; the latter two parameters become important only for small types ($D < 20$ mm) or viscous liquids ($\nu > 10^{-4}$ m^2/s), respectively. For the case that these parameters are important, various corrections on (1) exist in the literature (see for instance Fabre and Liné, 1992). In (1), the distribution parameter for the Taylor bubble, C_{TB}, accounts for the fact that in upward flow the bubble rises with a velocity U_0 relative to the centreline velocity of the pipe, which for a turbulent single-phase pipe flow exceeds the bulk velocity by some 20%; thus $C_{TB} = 1.2$. Measurements of the velocity profile in front of the Taylor bubble nose confirm this result (Polonsky et al., 1999b). In order to observe a stationary Taylor bubble, we would need a frame of reference rising upward with a velocity U_{TB}. The (downward) bulk velocity U_{SL} relative to the observer then would become

$$U_{SL} = U_{TB} - U_L = U_0 + 0.2U_L \quad \text{or} \quad U_L = (U_{SL} - U_0)/0.2. \tag{2}$$

In our experiments, we supply a span of liquid bulk velocities relative to the Taylor bubbles, which, using (2), get a physical interpretation. It means that the lowest possible bulk velocity is U_0, which mimics the flow relative to a bubble rising through stagnant liquid. Increasing the liquid velocity beyond U_0 then mimics a bubble rising through co-flowing liquid, with the increment as in (2).

We have performed experiments for three different liquid velocities as given in Table 1. The first three columns show the liquid velocity, the corresponding Taylor bubble Froude number, $Fr_{TB} = U_{SL}/U_0$, and the 'simulated' liquid velocity for a rising bubble flow, U_L. We have considered to simulate a Taylor bubble rising in stagnant liquid ($Fr_{TB} = 1$), and in co-flowing liquid ($Fr_{TB} = 1.2$ and 1.4). For comparison, we give the same parameters for the three literature experiments described in Section 1. We see that in these papers the Froude number is much larger than 1, indicating that they simulate Taylor bubbles rising through (fast) co-flowing liquid. In

Table 1
Bulk velocity in the set-up (1) and corresponding Froude number (2); simulated slug-flow bulk velocity (3)

(1)	(2)	(3)	Riiser et al. (1992)			Bacon et al. (1995)			Su and Metcalfe (1997)		
U_{SL} (m/s)	Fr_{TB} (−)	U_L (m/s)	U_{SL}	Fr_{TB}	U_L	U_{SL}	Fr_{TB}	U_L	U_{SL}	Fr_{TB}	U_L
0.342	1.00	0.00	0.43	1.77	0.93	0.52	2.0	1.3	0.49	2.0	1.2
0.409	1.20	0.34	(^{X})			0.72	2.8	2.3	0.61	2.5	1.8
0.478	1.40	0.68				0.83	3.2	2.9			
						0.93	3.6	3.4			

The three columns on the right show the range of these parameters as given in the literature. In these cases a range of gas losses is measured. Riiser gives also data (^{X}) for U_{SL} varying from 0.2 to 0.5 m/s (thus Fr_{TB} varying from 0.82 till 2.05) at a fixed gas flow rate.

Riiser's paper, the velocity range at which the measurements were done (marked ^{X}) also contains $Fr_{TB} = 1$; no special attention is given to this flow condition, however.

Next to the liquid flowrate, the velocity profile and the turbulence might also be of importance. An appropriate velocity profile to mimic the flow of liquid around a Taylor bubble rising through a flowing liquid would be very difficult to obtain in the laboratory, since it is a concave profile with a velocity U_0 at the centre, and U_{TB} at the walls. The influence of the shape of the velocity profile on the film flow is likely to be very small, however, since the acceleration of the fluid passing the Taylor bubble nose quickly flattens the velocity profile of the flow entering the liquid film anyway. For this reason, we created a relatively flat profile of velocity U_{SL} upstream of the Taylor bubble that was used for all experiments.

When a Taylor bubble is rising through stagnant liquid, the flow approaching the bubble is laminar; when it rises through a co-flowing (low-viscosity) liquid the flow is turbulent. To account for such differences, we manipulated the downward flow with two different 'grids' (A and B). The distance between the grids and the bubble nose (bubble cap), L_N, was kept fixed at $2D$ to avoid the radial flow restriction in the grids influencing the average flow around the Taylor bubble nose. The two grids differ in their grid Reynolds number $Re_M = U_{SL}M/v$ with M the mesh size. Grid A is a hexagonally stacked drinking-straw package ($M_A = 3$ mm, solidity $= 0.26$) that is used also as a flow straightener. The turbulence level produced by it was not measured, but is expected to be low near the Taylor bubble nose, since the fine-scaled turbulence ($Re_{M_A} \approx 1 \times 10^3$) gives a fast decay, and the bubble is relatively far away ($L_N/M_A \approx 70$). Grid B is a hexagonally perforated metal plate ($M_B = 20$ mm, solidity $= 0.57$), that is used to produce a turbulent integral length scale (L_T) comparable to that of fully-developed pipe flow. Its turbulence has probably little decayed when reaching the Taylor bubble; Re_M is much higher ($Re_{M_B} \approx 7 \times 10^3$), and the distance is small ($L_N/M_B \approx 10$), indicating that the flow has just reached homogeneity (Batchelor, 1953). When in use, grid B is mounted 15 mm ($5M_A$) below grid A.

In Fig. 4 we show the velocity profile 10 cm ($1D$) below grid A measured using a Pitot-tube. We see that the profile is relatively flat in the inner 80% of the section, with probably turbulent boundary layers of about 1 cm wide. The profiles were integrated, reproducing the flowmeter value within 1%. We also see that the centreline velocity U_{CL}, which is determined here as the average over the inner 80% of the tube, is some 5% higher than U_{SL}.

The small cap at the end of the inlet tube is needed to help stabilising the bubble in three ways: firstly, the velocity in the centre of our tube, U_{CL}, has a small mismatch; the actual measured value

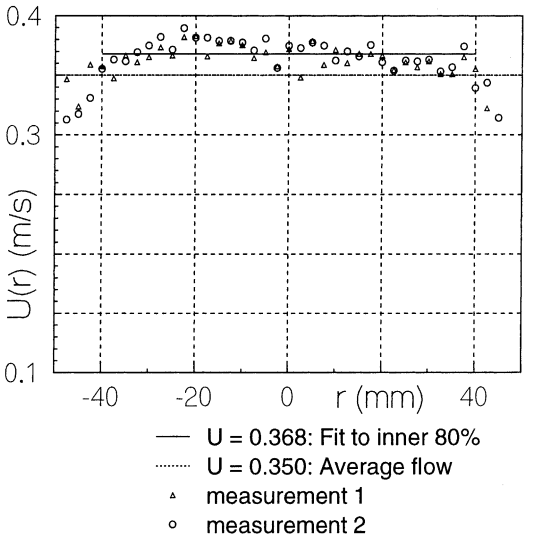

Fig. 4. Velocity profile measured at 10 cm ($1D$) below grid A, at the velocity $U_{SL} = 0.35$ m/s. The small asymmetry (RMS = 2.5% of average) is likely due to a small inhomogeneity in the grid.

($U_{CL} = 1.05U_{SL}$ as found above) is larger than during slug flow (then the velocity relative to the Taylor bubble nose should be U_0, as discussed above). Without the cap, the bubble would slowly move down. Also, the vertical position of the bubble nose is exactly fixed at $z = 0$ by the cap. Secondly, in a downward convex velocity profile the Taylor bubble nose is not very stable in the radial direction as was discussed in Section 1. Thirdly, the boundary layer growing along the air inlet tubelet upstream of the bubble nose easily detaches while decelerating towards the bubble nose. In preliminary experiments without the cap, large disturbances were visible on the film surface. With the cap, the boundary layer is stabilised again before contacting the film surface. The diameter of the cap ($0.4D$) was extended to the position where the outer flow has resumed the upstream velocity. With the cap, the film surface was observed to be much smoother, with only low-frequency waves that did not cause any entrainment. In this way, the influence of the no-slip condition on the first part of the film surface is considered to be minimised.

3. Observations

Our first experiment has been done at $Fr_{TB} = 1.0$ with the 'laminar' grid A. For short Taylor bubbles, up to 0.4 m length, the liquid film flows smoothly into the liquid column, entraining (nearly) no air. The wake of the Taylor bubble is very unsteady; the wake surface is on average nearly flat, but moves vigorously as also observed by Su and Metcalfe (1997) and, described in much more detail, by Polonsky et al. (1999a). Even though the motion is probably forced by the unsteadiness of vortices present in the wake, the motion of the surface seems to be a combination of simple resonant gravity waves. Especially the dominant mode, a standing wave that sloshes to and fro, is easily observed in the experiment. Its frequency compares with the theoretical frequency f_{SW} of a standing wave on a deep circular basin (Lamb, 1939):

$$f_{sw} = \frac{1}{2\pi}\sqrt{3.68g/D} \approx 3 \text{ Hz}. \quad (3)$$

From spectral analysis of the interface bottom shape, Polonsky et al. (1999a) found the frequency to be some 35% lower than the theoretical value, which they attribute to the fact that the boundary conditions as used to obtain the Lamb value would poorly apply to the flow conditions in the experiment.

When we slightly increase the bubble length (by blowing in some air), an intermittent entrainment process becomes visible at the Taylor bubble base, in which bubbles are produced now and then. These bubble creation events occur at random locations around the perimeter of the top of the liquid column into which the film flows. At locations of entrainment, the film surface is observed to be rougher than elsewhere. We call the Taylor bubble length at which this onset of entrainment occurs as L_{ON}. When L_{TB} is increased further, the frequency of the entrainment events increases, until at an excess length of about 0.50 m beyond L_{ON}, the entrainment process takes place continuously and all over the tube circumference. We also see then that the film surface above the point at which the film flows into the liquid column is rough around the whole circumference.

With increasing entrainment, the void fraction also increases both in the wake of the Taylor bubble and in the liquid column below it. The latter we measured (see Section 4); the former was observed visually. The three photographs in Figs. 5(a)–(c) show the conditions for low, intermediate and high void fraction. At low void fractions (left), the wake is hard to distinguish, but the entrainment is clearly visible. For intermediate voidages (centre), there is a clear separation

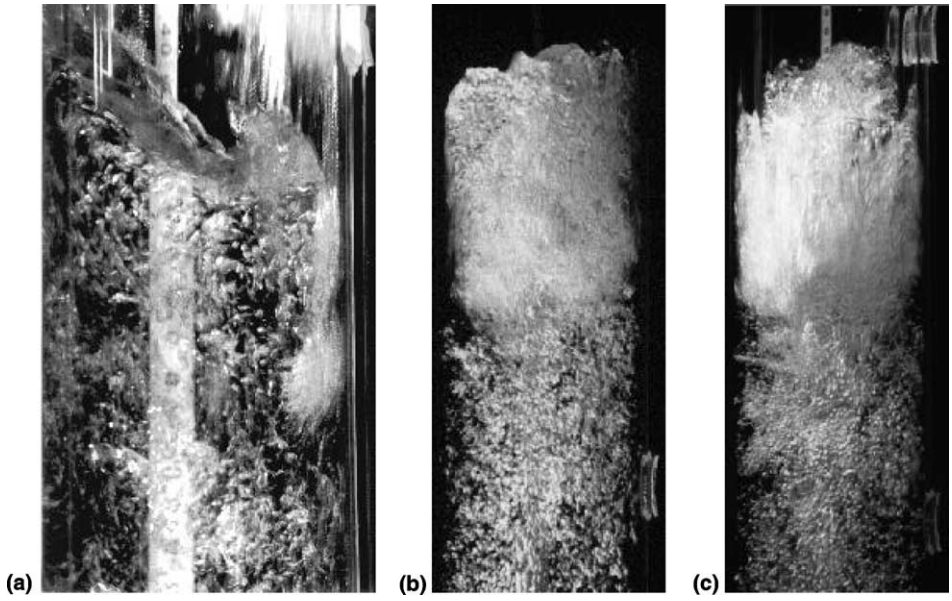

Fig. 5. Three flash photographs of the wake at: (a) a low, (b) an intermediate, (c) a high void fraction. On the left, the entrainment process is clearly visible from the formation of a single cloud of bubbles (in this case it was forced by disturbing the film flow).

between the recirculating wake and the bubbly flow below it. At a still higher void fraction, the wake becomes optically dense. From the photographs we see that the recirculating wake is about 1–1.5 tube diameters D long. This length did not vary much with either the liquid or the gas flow rate.

4. Measurements

At the same conditions as in Section 3, we have measured the gas loss, U_{SG}, as a function of Taylor bubble length, L_{TB}. The data points, as shown in Fig. 6, fall close onto a curve with little scatter around it. This curve will further on be called a *gas loss curve* $U_{SG}(z)$.

From this gas loss curve, we observe that below a Taylor bubble length of about 0.45 m the gas loss is very small. Beyond this length, the loss rate increases roughly linearly with L_{TB}. At about 1.0 m the loss increases more slowly until a loss maximum is found at about 1.2 m length. For still large L_{TB}, the gas loss decreases until an asymptotic value is reached that is about 10% smaller than the maximum loss. The length needed to reach the asymptotic gas loss is not completely clear but is seems to be some 2.0 m. Going from short to long Taylor bubbles, the gas loss curve can be characterised by three interesting features.

(a) An onset of entrainment.
(b) A gas loss maximum.
(c) An asymptotic gas loss.

Together with the gas loss we have determined the voidage profile $\alpha(z)$ from the pressure drop measurements along the liquid column. The results for the same measurements as above are shown in Figs. 7(a) and (b). In Fig. 7(a) the void fraction in the column $\alpha(z = L_{TB})$ is shown as a function of L_{TB}. We will call this the *void fraction curve*. Like in the gas loss curve, there is also a maximum in the void fraction curve. This maximum stays somewhat below 0.25, roughly the

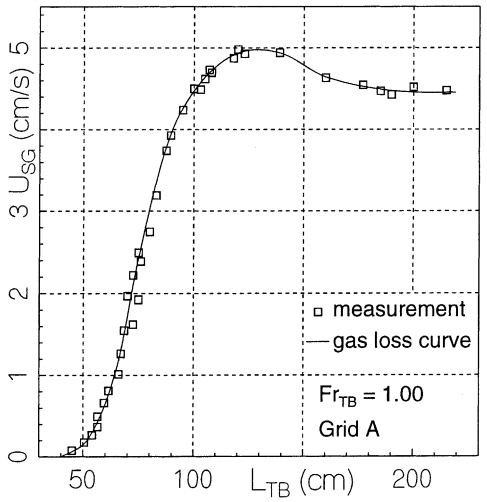

Fig. 6. Measurements of air loss from a Taylor bubble using laminar grid A, and a free-hand drawn gas loss curve.

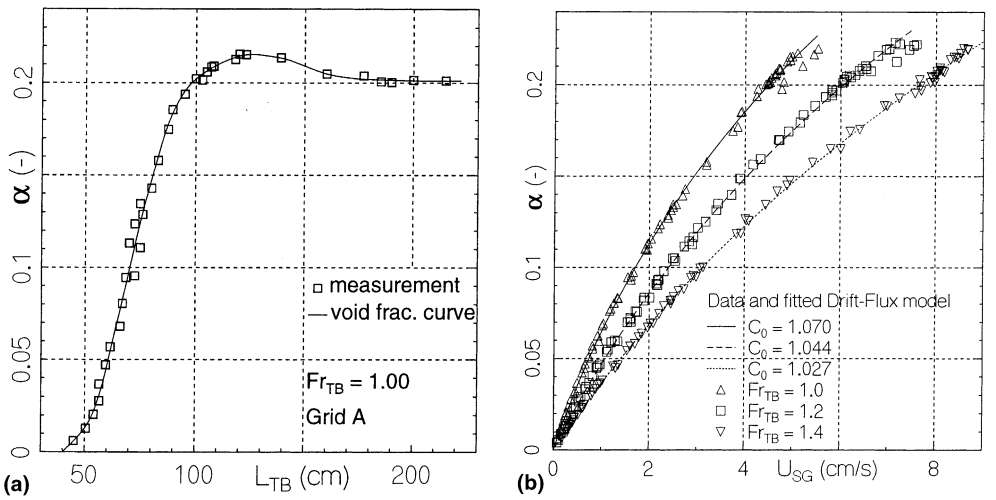

Fig. 7. Void fraction α in the liquid column below the Taylor bubble with laminar grid A. (a) α versus Taylor bubble length, with a free-hand drawn 'void fraction curve'. (b) α versus U_{SG} for all Fr_{TB} including drift-flux model with fitted C_0.

value from where bubble coalescence increases rapidly, and bubbly flow is likely to become unstable (for instance Matuszkiewicz et al., 1987). The asymptotic void fraction is still somewhat lower, a mere 0.2.

For the purpose of determining $\alpha(z)$, a fully developed bubbly flow can be characterised with sufficient accuracy by the one-dimensional drift-flux model as for instance described by Wallis (1969). In this model, there is a weakly non-linear relation between U_{SG} and α. In Fig. 7(b) we show U_{SG} against α in our experiment, together with the curve fits of the drift-flux model. The resulting 'distribution parameter' was found as decreasing from $C_0 = 1.07$ to 1.03 with Fr_{TB} increasing from 1.0 to 1.4, indicating that the radial void fraction profiles are relatively flat (Wallis, 1969). At the larger liquid flow velocities, the distribution parameters become even lower, but stay above 1.0.

To investigate if these values for C_0 are realistic, we needed to get more information on the radial distribution of the gas bubbles. For this we measured the radial void fraction profile, $\alpha(r)$, at $20D$ below the Taylor bubble nose, as is indicated in Fig. 2. We used a glass fibre probe that detects the phase (liquid or gas) from the refractive index of the medium contacting the fibre tip. The 0.1 mm diameter fibre is led through a traversable 1.2 mm diameter stainless steel tubelet pointing in the upstream flow direction. The local void fraction is then determined from the fraction of time that the tip is dry during 5 min measurement time. We applied five different gas flow rates, leading to average void fractions $\alpha(z = L_{TB})$ ranging from (0.03–0.16). The distance below the Taylor bubble wake was not constant because of the increasing Taylor bubble length with U_{SG}. Yet even at the largest Taylor bubble, the probe was still $12D$ below the Taylor bubble bottom, indicating that the distribution is already fully developed (van Hout et al., 1992). In the central region, the curves we measured were flat within measuring accuracy. The results near the two opposite tube walls are shown in Fig. 8. We see that for α below 0.05, the profiles decrease towards the wall. For higher α the radial profiles first show a slight peak some 5 mm away from

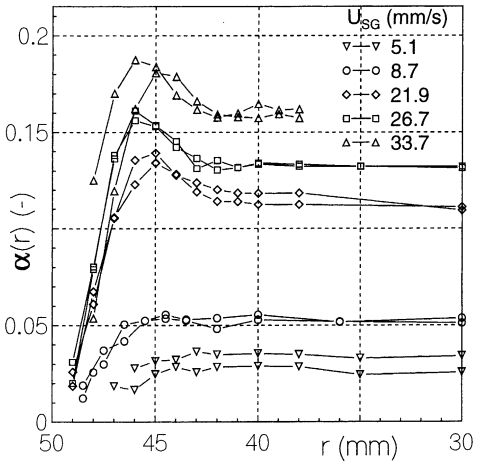

Fig. 8. Air loss for short Taylor bubbles for two grids (A full and B open symbols) and three liquid flow rates.

the wall, before decreasing as well. However, the large flat part in the tube centre confirms that a distribution parameter close to 1 is to be expected.

In the following we will discuss the properties of the gas loss and the void fraction curves for three liquid flow rates (corresponding to Froude numbers $Fr_{TB} = 1.0, 1.2$ and 1.4) and both laminar and turbulent upstream flow conditions (grids A and B). We found that in a qualitative manner, all these curves have characteristics more or less similar to those discussed above.

4.1. Small Taylor bubbles

In Fig. 9 we show the Taylor bubble lengths as measured for low gas losses (U_{SG} versus L_{TB}) for six flow conditions: three liquid velocities (marked with different symbols), and two upstream turbulence grids (indicated with full (grid 'A') and open (grid 'B') symbols).

There is a clear trend that increasing either the turbulence intensity or the liquid flow rate leads to a shorter Taylor bubble for the same entrainment rate. For gas losses not too close to zero entrainment, say $U_{SG} > 1$ cm/s, the gas loss increases linearly with L_{TB}, or dU_{SG}/dL_{TB} is constant for all curves. Before this region of linear increase is reached, the loss curves for grid A differ quite from those for grid B. The laminar grid A causes a considerable entrainment only beyond an 'onset of entrainment' length, L_{ON}, found by extrapolating the linear loss curve to the $U_{SG} = 0$ axis. For short Taylor bubbles, the turbulent grid B causes a slowly increasing entrainment. Yet, at a certain length, the loss curve shows a deflection point L_{DEF}, beyond which the entrainment increases linearly similar to that in the loss curves for grid A. We can explain these observations by proposing the following speculative mechanism for entrainment.

We suppose entrainment to occur only when the intensity of the turbulent velocity fluctuations in the film flow is sufficiently strong to provoke it. We suggest the entrainment rate to be proportional to both the velocity with which the film flow enters the Taylor bubble wake, and the intensity of the turbulent velocity fluctuations in the film. In this concept, for short L_{TB} the entrainment process is governed by the turbulence present in the flow upstream of the bubble; for

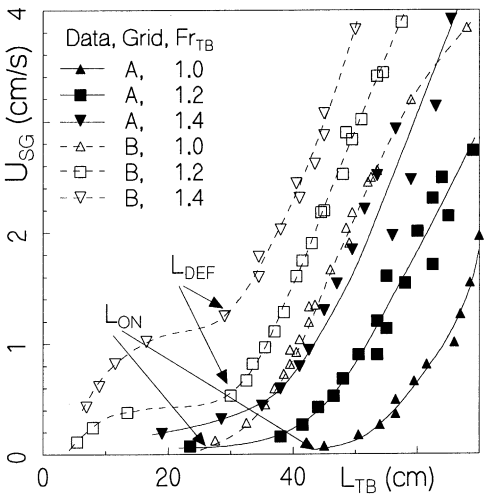

Fig. 9. Air loss for short Taylor bubbles for two grids (A full and B open symbols) and three liquid flow rates.

large L_{TB} by the wall shear-generated turbulence. In the latter case, it should not depend on the initial turbulence any more.

This hypothesis could explain why the 'turbulent' grid B provokes entrainment at short Taylor bubbles, whereas the 'laminar' grid A does not: the turbulence produced with grid B is strong enough to provoke the entrainment process. Although the turbulent fluctuations are reduced while the film is accelerated, (as described already by Prandtl, 1933), the increasing film velocity could still result in an increasing entrainment rate with Taylor bubble length. Further increase of Taylor bubble length gives also an increasing wall-shear stress. Beyond a certain film length the advected grid turbulence gets weaker than the turbulence generated by the wall shear. From this length on, it is the wall shear-generated turbulence that governs the entrainment process. This point of transition is visible in the gas loss curve. When the turbulence is strong, the transition is relatively early, as for grid B. If there is little or no grid turbulence, transition is relatively late and L_{DEF} is on the zero entrainment axis, as for grid A.

It should be clear that the entrainment mechanism proposed here is only a hypothesis and needs further study.

4.2. Large Taylor bubbles

In Fig. 10 we show the influence of the upstream turbulence on the void fraction α in the liquid column for $Fr_{TB} = 0.1$, and L_{TB} ranging from 0.2 to 2.2 m. As noted above, the two curves for the grids A and B behave differently for small bubble lengths, but rise roughly parallel. They approach each other for $L_{TB} = 1$ m; for larger L_{TB} they collapse. We see that at the void fraction maximum around $L_{TB} = 1.2$ m, the influence of the upstream turbulence on the entrainment has nearly vanished, even though the entrainment is not fully developed yet. For both curves the asymptotic α is the same; it takes an L_{TB} of some 2.0 m to reach this. We should note, however, that the number of data points is quite limited, especially for grid B.

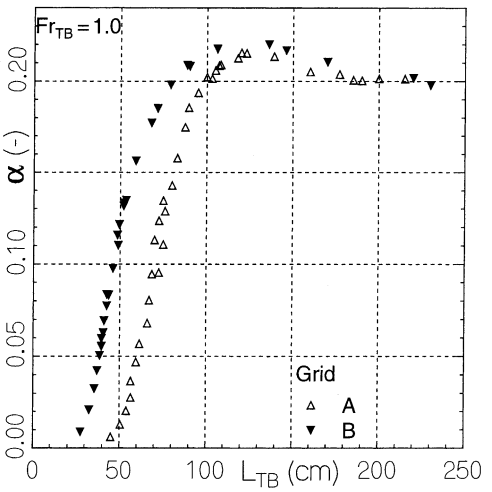

Fig. 10. The voidage α in the liquid column for two grids at $Fr_{TB} = 1.0$. The onset of entrainment is influenced by the upstream turbulence, whereas the maximum and the asymptote are unaltered.

The results for U_{SG} and α with both grids and all three Fr_{TB} are collected in Figs. 11(a)–(d). The gas loss increases with increasing liquid flow rate (Figs. 11(a) and (c)), but the shapes of the loss curves remain the same. The entrainment maxima occur at an L_{TB} of about 1.1–1.2 m for all flow conditions. The persistence of the entrainment maximum shows that it is hardly influenced by the flow conditions. The corresponding void fractions curves (Figs. 11(b) and (d)) collapse for L_{TB} larger than about 1 m. Thus, the voidage is hardly dependent on the liquid flow rate.

As suggested while discussing the entrainment process, we speculate the entrainment rate to be proportional to the film velocity and the strength of the turbulent velocity fluctuations in the film. One would expect both to rise with L_{TB} from small at the bubble top to a constant value after the film flow has become fully developed. Therefore, one would expect the entrainment to rise monotonically as well. As we see in Fig. 11, the gas loss and the void fraction curves yet all show a maximum, followed by a slow decline.

We see from Figs. 11(a) and (c) that for both grids the gas loss maximum becomes less pronounced for higher Fr_{TB}. For $Fr_{TB} = 1.0$, the overshoot is about 15%; for $Fr_{TB} = 1.4$, it is merely 5%. From this trend we may suggest that by further increasing the liquid flow rate, the gas loss maximum will disappear. However, the limited amount of data and the lack of full insight into the entrainment mechanism make a firm statement on this impossible.

4.3. Comparison with other data

Now we will discuss the similarities and differences between our results and those described in the literature, i.e., Riiser et al. (1992), Bacon et al. (1995) and Su and Metcalfe (1997).

In all experiments including ours, the entrainment flux increases with L_{TB} starting from little or none to a certain value. In three of the experiments, a fully developed film is just or nearly reached at the largest L_{TB}; Riiser studies only relatively short bubbles, in which the film flow is still far

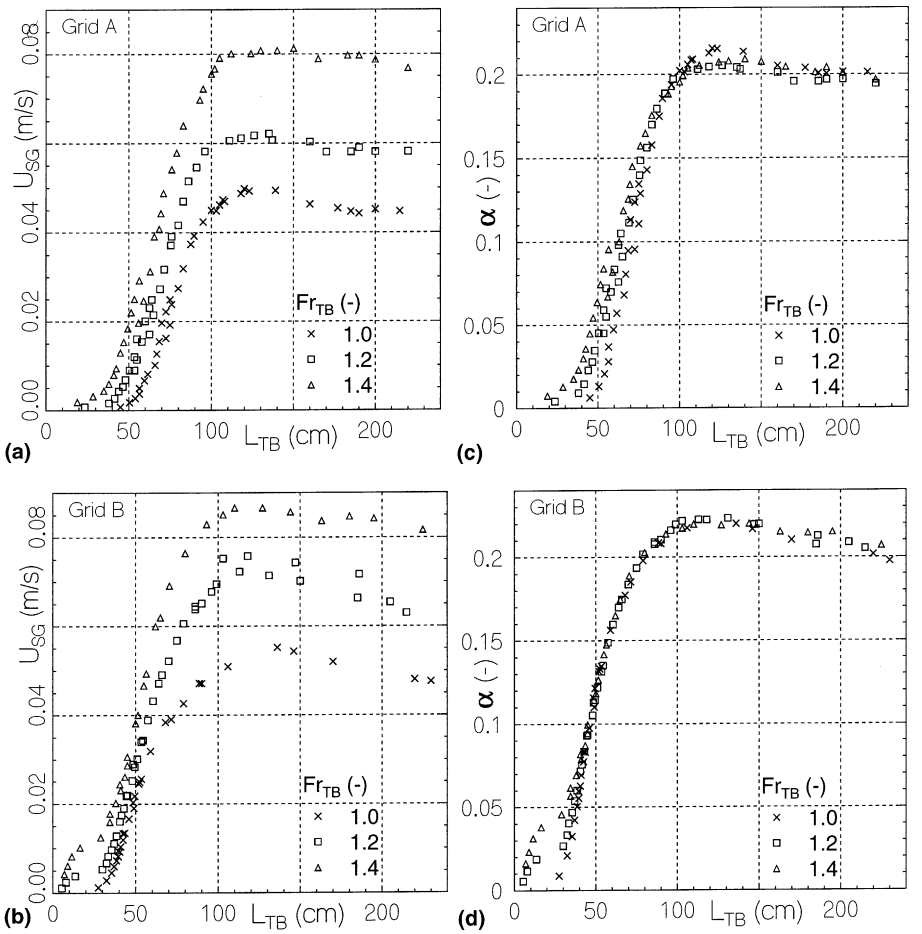

Fig. 11. Gas loss U_{SG} from (left), and void fraction α below (right) a Taylor bubble for the three different liquid flow rates. (a, c) grid A to give laminar inflow; (b, d) grid B to give turbulent inflow.

away from fully developed. The way in which the measured curves approach the final state is quite different, however.

A point to consider is the tube diameter D. We chose a fairly large value, as was discussed in Section 1, since for small tubes the free rise velocity of dispersed bubbles in water (the liquid used by all) is close to the free rise velocity of a Taylor bubble; as a result small bubbles can hardly be swept away from the Taylor bubble wake (Taitel et al., 1980), and a large re-coalescence is to be expected (Andreussi and Bendiksen, 1989). The three literature papers consider a Taylor bubble in tubes ranging from $D = 51$ to 58 mm, thus the re-coalescence could be large. Especially, Riiser's experiment operated at low liquid velocities may have been influenced by re-coalescence. With our $D = 100$ mm, we likely stay further away from a very large re-coalescence process. This is why we can apply the low liquid flow rate needed to simulate Taylor bubbles rising through stagnant liquid. Yet even then re-coalescence may still be relevant. Using a different measurement technique (Delfos et al., 2001), we found the fraction of the entrained gas that re-coalesces back into

the Taylor bubble to increase from 10% at small to about 40% at high gas entrainment rates. A further study of re-coalescence is, however, still needed.

The paper by Riiser et al. (1992) gives a single gas loss curve for $Fr_{TB} = 1.8$ for relatively small L_{TB}. These measurements resemble our gas loss curve for a 'turbulent' grid with $Fr_{TB} = 1.4$. Since in their experiment the liquid film flow emerges from a narrow annulus, we may expect it to have already a considerable turbulence level, which makes our comparison with the turbulent grid B reasonable. We hypothesised in Section 4.1 that entrainment is initially governed by upstream turbulence and only later on by wall shear-induced turbulence. Riiser's data support this hypothesis since they show a clear regime change at $L_{DEF} = 0.20$ m.

The paper by Bacon et al. (1995) gives gas loss curves for four different U_{SL}. All four show an onset of entrainment, decreasing from $L_{ON} = 0.15$ to 0.05 m for increasing U_{SL}. Their data show a continuous growth of air loss with L_{TB}. While their gas loss still slowly increases with L_{TB} even at the largest $L_{TB} = 1.2$ m, a fully developed flow seems not to have been reached yet. In our own data, we see as well that the film flow is not developed until a very large length, i.e., about $L_{TB} = 2.0$ m.

The paper by Su and Metcalfe (1997) gives gas loss curves for two different U_{SL}. In their data we see a clear onset of entrainment; $L_{ON} = 0.1$–0.2 m. After a fast rise in the first, say, 0.8 m, the next (single) data point is given only at $L_{TB} = 1.5$ m. We suspect that there is either a slight gas loss maximum or a constant gas loss level. However, in a length region where U_{SG} decreases with L_{TB}, the bubble length is unstable when the air feed flow comes from a high-pressure system (Delfos, 1996). Only in a system where the air inlet flow is controlled can measurements be done in such a region. It is interesting that if Su has a loss maximum, it is found at roughly the same L_{TB} as ours. It is also interesting to note that on average the *shapes* of their curves show trends very similar to ours.

Qualitatively, we have seen many resemblances and only a few differences. To make a quantitative comparison is still difficult. It is clear that there is still need of a physical model that explains the characteristics found by the various authors in a quantitative way.

5. Conclusion

We have presented an experimental set-up in which a Taylor bubble can be held stationary in a vertically downward flow while varying the liquid flow rate and some turbulence properties independently. We have presented photographs from the bubble nose and the bubble wake. We have measured the air loss U_{SG} from, and the gas volume fraction α below the bubble as a function of the bubble length L_{TB}. We conclude the following.

With photographs we have shown that the nose of our artificial, standing Taylor bubble resembles that of a freely rising bubble, and that of the theoretical shape following from potential flow theory. In previous experiments on stationary Taylor bubbles as reported in the literature, little attention was given to the Taylor bubble nose.

Photographs show that below the Taylor bubble base there is a strongly recirculating wake, with a length of about 1–1.5D, independent of the film entrance velocity or the film flow rate.

The Taylor bubble hardly loses air below a certain length L_{ON} which ranges from 0.3 m for turbulent to 0.5 m for laminar upstream flow. Beyond this length we have observed a highly

intermittent entrainment process, in which small clouds of bubbles are entrained from the Taylor bubble into its wake. Our experiments suggest that L_{ON} is related to the transition of the liquid film flow from laminar to turbulent.

Beyond L_{ON} the gas loss increases roughly linearly with L_{TB} until it reaches a maximum at $L_{TB} \approx 1.2$ m. Beyond that length, U_{SG} decreases slowly, until a fully developed state is reached at L_{TB} around 2 m. Then U_{SG} has shrunk some 5–15% relative to the maximum, the shrink decreasing with increasing U_{SL}.

The gas volume fraction in the liquid column $\alpha(z)$ determined from pressure drop measurements correlates well with the gas loss U_{SG} via the drift-flux model. The distribution parameter in this model, C_0, was found to decrease from 1.07 to 1.03 with increasing Fr_{TB}. Measured radial void fraction profiles $\alpha(r)$ at $Fr_{TB} = 1.0$ show a flat distribution in the inner 80% of the cross-section, with small peaks some 5 mm away from the wall at elevated average void fractions. These profiles support a value for C_0 of only a little above 1.0.

The gas loss from the Taylor bubble increases with increasing liquid flow rate. The void fraction in the liquid column below the bubble only slightly depends on Fr_{TB}, especially for Taylor bubbles larger than 1 m length.

Our data suggest that turbulence in the film plays an important role in the entrainment process.

6. Suggestions for further work

In our experiment, a natural transition to turbulent flow in the film surrounding the Taylor bubble is influenced by the upstream turbulence level. By using a trigger, for instance by a trip wire, one could make a more controlled transition.

For Taylor bubble lengths near and beyond the air loss maximum, our number of data points is limited. Also, these points show relatively much scatter due to the low bubble length stability there. Additional data points are needed to better establish the gas loss curves.

To further investigate the entrainment mechanism, this process ought to be studied both experimentally and theoretically. Information on the characteristics of the film velocity and the shape of the film surface are expected to be very important for this case.

Our measuring technique only measures the difference between the entrainment rate and the recoalescence rate. A technique that does separate the two (Delfos et al., 2001) suggests the recoalescence to strongly depend on the void fraction in the wake. The latter could be measured using properly calibrated optical probes or from the pressure drop over the wake (Delfos, 1996).

References

Andreussi, P., Bendiksen, K., 1989. An investigation of void fraction in liquid slugs for horizontal and inclined gas–liquid pipe-flow. Int. J. Multiphase Flow 15, 937–946.

Bacon, R.P., Scott, D.M., Thorpe, R.B., 1995. Large bubbles attached to spargers in downwards two-phase flow. Int. J. Multiphase Flow 21, 949–959.

Batchelor, G.K., 1953. The Theory of Homogeneous Turbulence. Cambridge University Press, Cambridge.

Delfos, R., 1996. Experiments on air entrainment from a stationary slug bubble in a vertical tube. Ph.D. thesis, Delft University of Technology.

Delfos, R., Alexanderson, M., Oliemans, R.V.A., 1993. Experimental simulation of entrainment behind Taylor-bubbles in vertical slug flow. In: Proceedings of the 6th International Conference on Multiphase Production, Cannes, France, pp. 323–332.

Delfos, R., Rops, C.M., Kockx, J.P., Nieuwstadt, F.T.M., 2001. Measurement of the re-coalescence flux into the rear of a Taylor bubble. Phys. Fluids 13.

Dukler, A.E., Fabre, J., 1992. Gas–liquid slug flow; knots and loose ends. In: Proceedings of the 3rd International Workshop on Two-Phase Fundamentals, ICL, London, pp. 1–66.

Dumitrescu, D.T., 1943. Strömung an einer Luftblase im senkrechten Rohr. Z. angew. Math. Mech. 23, 139–149.

Fabre, J., Liné, A., 1992. Modelling of two phase slug flow. Ann. Rev. Fluid. Mech 24, 21–46.

Fabre, J., Liné, A., Peresson, L., 1989. Two fluid/two flow pattern model for transient gas–liquid flow in pipes. In: Proceedings of the 4th International Conference on Multiphase Flow, Nice, France, pp. 269–284.

Fernandes, R.C., Semiat, R., Dukler, A.E., 1983. Hydrodynamic model for gas liquid slug flow in vertical tubes. AIChE J. 29, 981–989.

Lamb, H., 1939. Hydrodynamics, sixth ed. Cambridge University Press, Cambridge.

Mao, Z.-S., Dukler, A.E., 1989. An experimental study of gas–liquid slug flow. Exp. Fluids 8, 169–182.

Martin, C.S., 1976. Vertically downward two-phase slug flow. J. Fluids Eng., 715–722.

Matuszkiewicz, A., Flamand, J.C., Bourre, J.A., 1987. The bubble slug flow pattern transition and instabilities of void fraction waves. Int. J. Multiphase Flow 13, 199–217.

Nicklin, D.J., Wilkes, J.O., Davidson, J.F., 1962. Two-phase flow in vertical tubes. Trans. Inst. Chem. Engs. 40, 61–68.

Oliemans, R.V.A., 1990. Applied Multiphase Flows. Lecture notes, Delft University of Technology.

Polonsky, S., Barnea, D., Shemer, L., 1999a. Averaged and time-dependant characteristics of the motion of an elongated bubble in a vertical pipe. Int. J. Multiphase Flow 25, 795–812.

Polonsky, S., Shemer, L., Barnea, D., 1999b. The relation between the Taylor bubble motion and the velocity field ahead of it. Int. J. Multiphase Flow 25, 957–975.

Prandtl, L., 1933. Attaining a steady air stream in windtunnels, Report NACA TM 726.

Riiser, K., Fabre, J., Suzanne, C., 1992. Gas entrainment at the rear of a Taylor bubble. In: Proceedings of the European Two-Phase Flow Group Meeting, Stockholm, pp. 1–8.

Su, C., Metcalfe, R.W., 1997. Influences of liquid properties on gas entrainment at the bottom of a fixed bubble. In: Proceedings of the ASME Fluids Engineering Division Summer Meeting, Vancouver, pp. 1–7.

Taitel, Y., Barnea, D., Dukler, A.E., 1980. Modelling flow pattern transitions for steady upward gas–liquid flow in vertical tubes. AIChE J. 26, 345–354.

van Hout, R., Barnea, D., Shemer, L., 1992. Spatial distribution of void fraction within a liquid slug and some other related slug parameters. Int. J. Multiphase Flow 18, 831–845.

Wallis, G.R., 1969. One-Dimensional Two-Phase Flow. McGraw-Hill, New York.